Vol 460|30 July 2009|doi:10.1038/nature08198

ARTICLES

Crystal structure of the ATP-gated $P2X_4$ ion channel in the closed state

Toshimitsu Kawate[1], Jennifer Carlisle Michel[1], William T. Birdsong[1] & Eric Gouaux[1,2]

P2X receptors are cation-selective ion channels gated by extracellular ATP, and are implicated in diverse physiological processes, from synaptic transmission to inflammation to the sensing of taste and pain. Because P2X receptors are not related to other ion channel proteins of known structure, there is at present no molecular foundation for mechanisms of ligand-gating, allosteric modulation and ion permeation. Here we present crystal structures of the zebrafish $P2X_4$ receptor in its closed, resting state. The chalice-shaped, trimeric receptor is knit together by subunit–subunit contacts implicated in ion channel gating and receptor assembly. Extracellular domains, rich in β-strands, have large acidic patches that may attract cations, through fenestrations, to vestibules near the ion channel. In the transmembrane pore, the 'gate' is defined by an ~8 Å slab of protein. We define the location of three non-canonical, intersubunit ATP-binding sites, and suggest that ATP binding promotes subunit rearrangement and ion channel opening.

ATP is most commonly known as the vital carrier of free energy, having multifaceted roles in energy metabolism, biosynthesis and intracellular signal transduction. A non-canonical role for ATP in extracellular signal transduction emerged from studies showing that ATP is released from sensory nerves and promotes vasodilatation[1]. Subsequently, the concept of ATP-mediated signalling, termed purinergic signalling, was provided by Burnstock as a ubiquitous mechanism for extracellular communication[2]. Interest in this field redoubled after molecular cloning and characterization of two different ATP receptors: ionotropic P2X, and G-protein-coupled P2Y receptors[3–6]. Although the physiological importance of purinergic signalling is now generally accepted[7], the determination of the molecular mechanisms of ATP binding and the subsequent signal transduction has been hindered by the absence of high-resolution structures for any ATP receptors.

Ionotropic P2X receptors are widely distributed throughout the human body and participate in diverse physiological processes, from the nervous system to the immune system[8]. In the central nervous system, presynaptic neurons expressing P2X receptors enhance the release of neurotransmitters such as glutamate[9,10] and GABA (γ-aminobutyric acid)[11,12], whereas expression in postsynaptic neurons is required to evoke an ATP-induced postsynaptic current[13,14]. In the peripheral nervous system, afferent neurons carrying P2X receptors sense a variety of stimuli, such as taste[15], pain[16,17] and distention of the bladder[18]. Furthermore, P2X-receptor-deficient mice demonstrate the involvement of these receptors in blood pressure regulation and vascular remodelling, autoregulation of blood flow in the retina, and interleukin-1β production from macrophages[19–22]. Because P2X receptors are integral to many signal transduction pathways, it is perhaps not surprising that the dysfunction of P2X-receptor-mediated signalling is implicated in cancer[23] and inflammatory[24], cardiovascular, and neuronal diseases. P2X receptors are therefore promising targets for new therapeutic agents.

P2X receptors are cation permeable, ATP-gated ion channels derived from seven different subtypes ($P2X_{1–7}$) found only in eukaryotes[25]. Intact receptors are composed of three subunits assembled as either homomeric or heteromeric complexes contingent on the specific subunits and the cellular context[26–29]. Gating kinetics and pharmacology vary widely between different homomeric and heteromeric receptor assemblages. Whereas homomeric $P2X_1$ receptors exhibit rapid, nearly complete desensitization and high sensitivity to suramin and pyridoxalphosphate-6-azophenyl-2',4'-disulphonic acid (PPADS), homomeric $P2X_4$ receptors show slow, incomplete desensitization and insensitivity to common P2X receptor antagonists[30]. Secondary structure prediction and hydropathy plots indicate that each subunit has two transmembrane segments arranged such that the intracellular domain is formed by the amino and the carboxy termini. Although the transmembrane topologies of P2X receptors are similar to acid-sensing ion channels (ASICs, also known as ACCNs), epithelial sodium channels (ENaCs), and degenerin channels (DEGs)[31], there is little, if any, relationship between their primary amino acid sequences.

Ascertaining the structure of a P2X receptor will not only elaborate on the architecture of this important class of ligand-gated ion channels and, thus, form the basis for molecular mechanisms of function, but it will also provide new insights into the molecular principles of agonist and antagonist binding, in turn spurring the design of new therapeutic agents. Here we show the crystal structure of a zebrafish $P2X_4$ receptor at 3.1 Å resolution, verifying that these receptors are trimers with previously unseen subunit folds and non-canonical ATP-binding sites. The closed transmembrane pore, consistent with crystallization of the receptor in the absence of ATP, defines the ion channel gate in a closed, resting state.

Crystallization and structure determination

P2X receptors tend to aggregate or dissociate in the presence of detergents commonly used for crystallization (Supplementary Fig. 1). We therefore used fluorescence-detection size-exclusion chromatography (FSEC) to rapidly and efficiently evaluate the stability and monodispersity of 35 P2X orthologues expressed in transiently transfected HEK293 cells[32]. The zebrafish $P2X_{4.1}$ receptor (encoded by *p2rx4a*; $P2X_4$) emerged as a promising candidate for crystallization trials because it has a sharp and symmetrical elution profile (Fig. 1d, grey trace). The full-length zebrafish $P2X_4$ receptor is activated by ATP with an effector concentration for half-maximum response (EC_{50}) of ~800 μM (Fig. 1a and Supplementary Fig. 2a)[33]. To improve crystallization behaviour, however, we analysed a series of N and C termini

[1]Vollum Institute, [2]Howard Hughes Medical Institute, Oregon Health and Science University, 3181 Southwest Sam Jackson Park Road, Oregon 97239, USA.

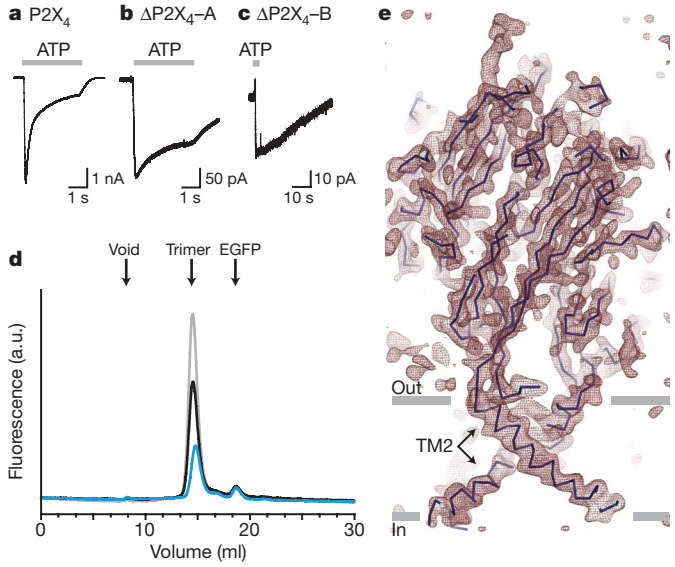

Figure 1 | A functional $P2X_4$ receptor for structural studies. **a**–**c**, Whole cell recordings of ATP-evoked current (1 mM, 3 s, grey bars) from the full-length $P2X_4$-EGFP construct (**a**), the $\Delta P2X_4$-EGFP-A construct (**b**), and the $\Delta P2X_4$-EGFP-B construct (**c**). **d**, FSEC profiles for $P2X_{4.1}$-EGFP (grey), $\Delta P2X_4$-EGFP-A (black), and $\Delta P2X_4$-EGFP-B (blue) expressed in tsA201 cells. The arrows indicate the estimated elution position of the void volume, the $P2X_4$-EGFP receptor (trimer) and free EGFP. a.u., arbitrary units. **e**, $2F_o - F_c$ electron density map contoured at 1.2σ. The blue line represents the Cα trace and the grey bars suggest the boundaries of the outer (out) and inner (in) leaflets of the membrane bilayer. The featured slice depicts TM2 helices but not TM1.

deletion mutants, settling on a minimal yet functional construct ($\Delta P2X_4$-A; Fig. 1d, black trace). Further optimization to avoid non-native disulphide bond formation and to reduce heterogeneity resulting from glycosylation yielded a derivative of $\Delta P2X_4$-A containing three point mutations (Cys51Phe/Asn78Lys/Asn187Arg; termed $\Delta P2X_4$-B; Fig. 1d, blue trace). Electrophysiological experiments showed that both $\Delta P2X_4$-A and -B are activated by 1 mM ATP (Fig. 1b, c), although the peak current amplitudes are smaller than those recorded from the full-length receptor (Fig. 1a)—an observation consistent with the lower expression levels of the mutants (Fig. 1d and Supplementary Fig. 2b–d). The $\Delta P2X_4$-A structure was solved by single-wavelength anomalous diffraction (SAD) using a gadolinium derivative, and the $\Delta P2X_4$-B structure was solved by molecular replacement (Supplementary Tables 1 and 2). Because the $\Delta P2X_4$-B crystals diffract to higher resolution than those formed from the $\Delta P2X_4$-A construct, we used the $\Delta P2X_4$-B structure in most of the analysis reported here.

Architecture

The homotrimeric zebrafish $P2X_4$ receptor has a chalice-like shape, with the large extracellular domain protruding ~70 Å above the membrane plane, and the comparatively smaller transmembrane stem extending ~28 Å through the membrane (Fig. 2a). In the $\Delta P2X_4$-A receptor complex each of the three crystallographically independent subunits adopts a similar conformation (Supplementary Fig. 7), and in the $\Delta P2X_4$-B structure the subunits are related by the crystallographic three-fold axis of symmetry passing through the receptor centre, perpendicular to the putative membrane plane (Supplementary Fig. 8).

The shape of the transmembrane region is reminiscent of an hourglass and is formed by six transmembrane helices, two from each of the three subunits. Within a subunit, the transmembrane helices are oriented approximately antiparallel to one another and are angled nearly 45° from the membrane normal. The inner TM2 helices cross each other about halfway across their membrane-spanning lengths, constricting the transmembrane pore and defining the closed, resting state of the channel (Fig. 1e). At the cytoplasmic termini of TM1 and TM2 the electron density is weak and we were not able to fit all of the residues to electron density features.

In contrast to the left-handed twist of the transmembrane helices, as seen from the cytoplasmic termini, the extracellular region of each subunit wraps around its neighbour with a right-handed twist, gripping adjacent subunits with extensive contact interfaces (Fig. 2a). The large extracellular domain, when viewed perpendicular to the crystallographic three-fold axis of symmetry, has a corrugated profile, replete with protruding *N*-linked glycosylation moieties. Seen parallel to the three-fold axis, the extracellular domain is shaped like an equilateral triangle (Fig. 2b). Although the transmembrane topology of P2X receptors is similar to that of ASICs and other members of the ENaC/DEG superfamily, the fold of the extracellular domains and the corresponding trimeric quaternary architecture is entirely different from ASICs, tetrameric ionotropic glutamate receptors and pentameric Cys-loop receptors.

Subunit fold and interfaces

The $P2X_4$ subunit resembles the shape of a dolphin, with the transmembrane helices and the extracellular region akin to the flukes and the upper body, respectively (Fig. 3a). The central architecture of the extracellular body domain is characterized by a transthyretin-like β-sandwich motif[34]. This domain appears structurally rigid and perhaps even resistant to conformational changes because the two β-sheets in the β-sandwich are knitted together by extensive contacts. Interestingly, the upper regions of the core β-sheets in the body domain contact neighbouring subunits, whereas there are no contacts between adjacent subunits at the base of the extracellular domain, proximal to the transmembrane domain. This conformation may allow the transmembrane helices, which are connected directly to the lower region of the body domain, the latitude to move to an open conformation after ligand-induced rearrangement of the upper regions. Attached to the body domain are the head domain and three structurally different elements: the dorsal fin, the right flipper and the left flipper. The head domain adopts a fold similar to an oligosaccharide-binding protein[35], and is defined by three antiparallel β-strands and one α-helix. Electron density is weak between Lys 136 and Asp 141, and we have introduced a corresponding break in the polypeptide chain. We find that all ten conserved cysteine residues in the extracellular region form pairings previously predicted by mutagenesis and electrophysiological studies[36,37] (Supplementary Fig. 9).

Subunit–subunit interactions are largely mediated by the extracellular domains, and a single subunit buries ~3,750 $Å^2$ of surface area upon trimer formation. The three major subunit–subunit interfaces are: body-to-body, head-to-body, and left-flipper-to-dorsal-fin (Fig. 3b). On the one hand, the residues forming the core β-sheets in the body domain are highly conserved, suggesting that the body-to-body interactions represent contacts common to all P2X receptors. On the other hand, the residues in the head, the left flipper, and the dorsal fin are less conserved (Supplementary Figs 3 and 10). We speculate that the head-to-body and the left-flipper-to-dorsal-fin interactions may encode some of the chemical and structural information that guides assembly of homomeric or heteromeric receptors. Subunit–subunit contacts are also probably involved in receptor function and, consistent with this hypothesis, experiments have shown that a single mutation in the left flipper of the $P2X_3$ receptor, Asp266Ala (Asp 283 in zebrafish $P2X_4$), considerably slows the rate of receptor desensitization[38]. A plausible explanation for the lack of function in homotrimeric $P2X_6$ receptors is that owing to ~9 missing residues in the left flipper, subunit–subunit contacts are compromised, decoupling agonist binding from ion channel gating.

Closed, resting state

The ion channel domain consists of three TM2 helices arranged around the three-fold axis of molecular symmetry, positioned to define most of the ion conducting pathway and surrounded by

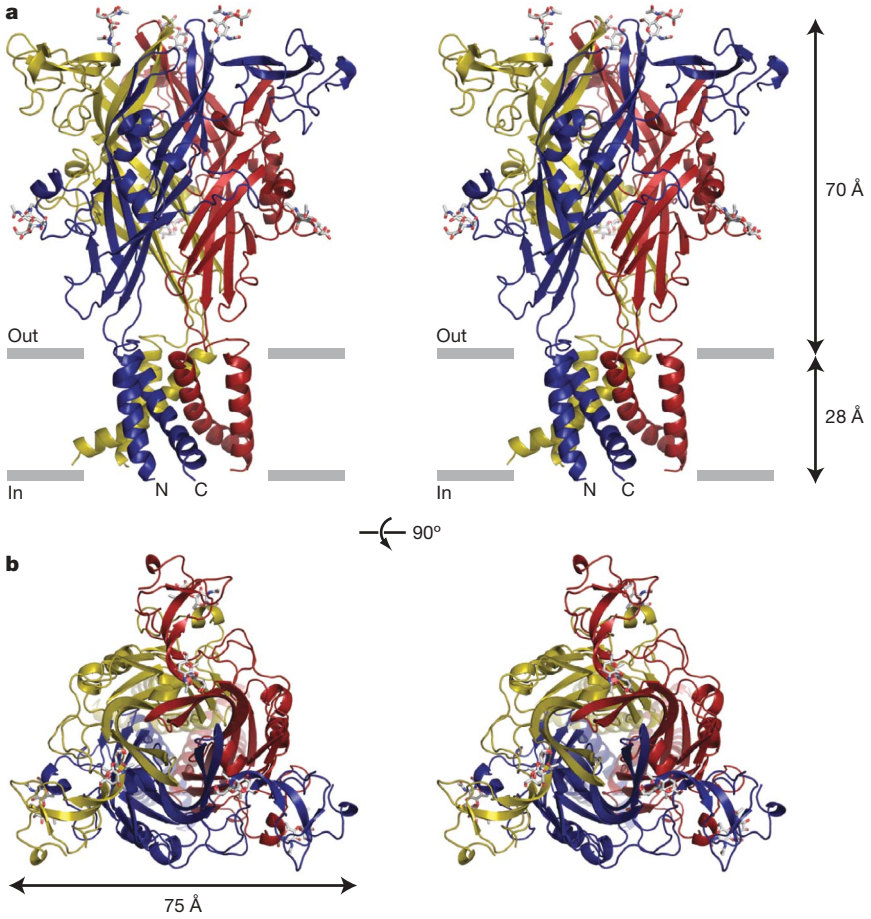

Figure 2 | The architecture of P2X receptors. **a**, Stereoview of the homotrimeric $\Delta P2X_4$ structure viewed parallel to the membrane. Each subunit is depicted in a different colour. NAG and glycosylated asparagine residues are shown in stick representation. The grey bars suggest the boundaries of the outer (out) and inner (in) leaflets of the membrane bilayer. **b**, Stereoview of the homotrimeric $\Delta P2X_4$ structure parallel to the molecular three-fold axis from the extracellular side of the membrane.

three peripheral TM1 helices (Fig. 4). A solvent-accessible surface representation clearly shows that the extracellular vestibule extends only a fraction of the distance across the membrane bilayer, to residues Leu 340 and Asn 341. On the cytoplasmic side of this occlusion, probably 5–10 Å from bulk intracellular solution, there is a solvent-accessible intracellular vestibule. Because the receptor was crystallized in an agonist-free, apo state, and because the putative ion permeation pathway is unambiguously occluded, the present structure provides an atomic model for the closed, resting state of P2X receptors.

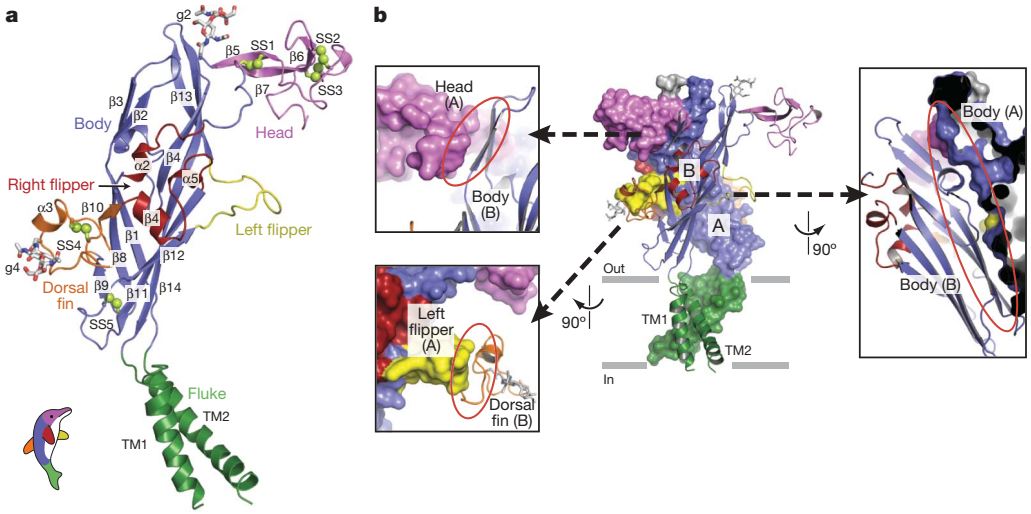

Figure 3 | Subunit fold and intersubunit contacts. **a**, The $\Delta P2X_4$ subunit has a dolphin-like shape. α-helices (TM1–2 and α2–5), β-strands (β1–14), disulphide bonds (SS1–5), and attached glycans (g2 and g4) are indicated. **b**, Interface of two adjacent subunits. Subunits A and B are shown in a solvent-accessible surface model and a cartoon representation, respectively. The three major subunit–subunit interfaces are emphasized in different panels in which the red ellipses highlight the contacts between the two subunits. Models are coloured according to domains as in panel **a**.

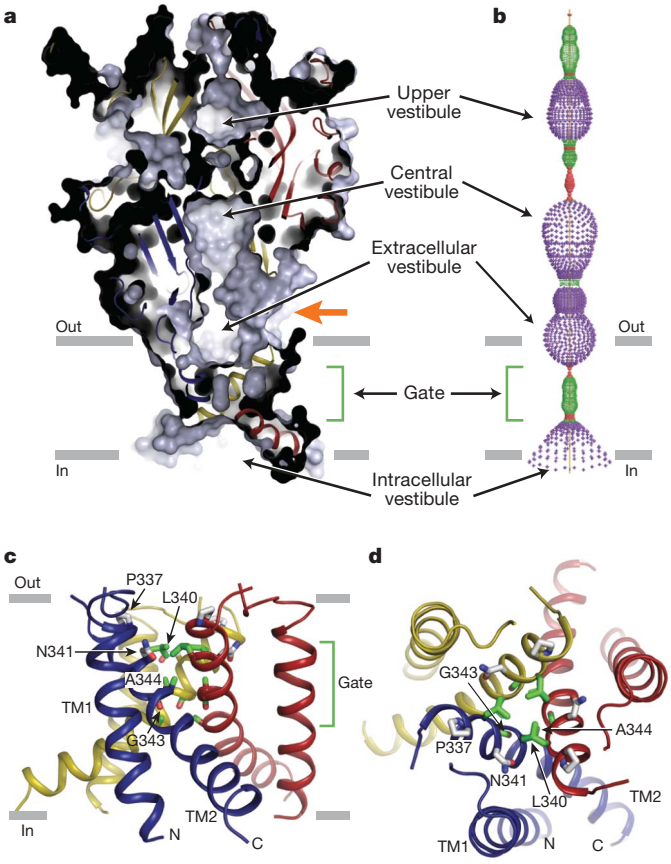

Figure 4 | Closed, resting conformation. **a**, A sagittal section reveals a closed conformation of the pore and shows that the gate is located about halfway across the membrane bilayer. Four vestibules (upper, central, extracellular and intracellular vestibules) are located on the molecular three-fold axis, with the extracellular vestibule connected to the bulk solution through a fenestration (orange arrow). **b**, Pore-lining surface calculated by the HOLE[49] program. Each colour represents a different radius range measured from the receptor centre (red: <1.15 Å, green: 1.15–2.3 Å, and purple: >2.3 Å). **c**, Cartoon representations of the transmembrane domain viewed parallel to the membrane plane. Phe 337 and Asn 341 are shown in grey, and potential gate residues (Leu 340, Gly 343 and Ala 344) are shown in green. **d**, Transmembrane domain viewed perpendicular to the membrane plane.

Ion channel access

Inspection of the zebrafish $P2X_4$ structure suggests two pathways by which ions in extracellular solution might access the transmembrane ion channel. The first pathway is through any of three fenestrations located directly above the transmembrane domains, proximal to the extracellular leaflet of the membrane bilayer (Fig. 4a, orange arrow). With openings as large as ~8 Å in diameter, these fenestrations should readily allow Na^+, K^+ and Ca^{2+} ions to access the channel. A second possible pathway runs the length of the extracellular domain, along the three-fold axis of symmetry and through two conspicuous vestibules rich in acidic residues (Fig. 4a, b). In this apo, closed-state structure the constrictions flanking the upper vestibule are too narrow for hydrated ions to pass (~2.3 Å). However, agonist binding may induce conformational changes between subunits, expanding these constrictions and, thus, enabling ions to access the transmembrane ion channel. On the cytoplasmic side of the ion channel, we propose that ions exit or enter the pore by the intracellular vestibule, an inverted cone-like structure that includes the conserved aspartic acid residue, Asp 357, a residue important to receptor assembly[39].

Ion channel gate

What are the solvent-accessible boundaries of the ion channel gate, and what residues or elements of protein structure define the gate? Viewed from the extracellular surface, residues Leu 340 and Asn 341 define the extracellular boundary of the ion channel gate, with the hydrophobic side chain of Leu 340 occluding the pore. On the opposite side of the membrane, the cytoplasmic gate is defined by Ala 347 and the side chain of Leu 346 (Fig. 4c, d and Supplementary Fig. 11). The 'centre' of the gate is Ala 344 and it defines the closest association of the TM2 helices. Therefore, the P2X receptor ion channel gate is primarily flanked by hydrophobic residues, includes about two turns of the TM2 α-helix, is composed of a slab of packed protein that is ~8 Å thick, and is consistent with recent cysteine-accessibility studies[40].

Ion selectivity

On the basis of the analysis of the current $P2X_4$ structure, together with the recently solved structure of a minimal functional chicken ASIC1 construct (ASIC1mfc)[41], we speculate on the molecular basis of cation selectivity in P2X receptors and suggest two distinct yet complementary mechanisms. First, the presence of several acidic residues in the central vestibule, immediately above the ion channel, together with Asp 59 and Asp 61 near the extracellular fenestrations, may not only enable the direct binding of cations, but may also create a long-range negative electrostatic potential that serves to concentrate cations near the extracellular entrance of the ion channel (Fig. 5g). Second, we suggest that permeant ions interact directly and specifically with the main-chain and side-chain oxygen atoms in the transmembrane ion channel. Although we have not yet determined the conducting, open channel structure, we speculate that the side-chain oxygen atom of Asn 341 may interact directly with permeant ions, perhaps in a similar manner to the interactions between Asp 433 and Cs^+ in the ASIC1mfc structure[41]. As ions progress towards the cytoplasm, main-chain carbonyl oxygen atoms from carbonyl groups slightly tipped off of the TM2 helix axis may participate in further protein–ion interactions.

Modulation by Gd^{3+}

To solve the structure of the $\Delta P2X_4$-A construct, we used a Gd^{3+} derivative and found four highly occupied sites. One site is located in the central vestibule, on the three-fold axis of non-crystallographic symmetry, and is coordinated by carboxylate groups of Glu 98 residues from each of the three subunits (Fig. 5a, c, d, g). The other three Gd^{3+} sites are located at the periphery of the receptor (one site for each subunit) and are coordinated by the carboxylate group of Asp 184 and the hydroxyl group of an *N*-acetyl-D-glucosamine (NAG) residue attached to Asn 187 (Fig. 5a, b, d). Because P2X receptors are commonly modulated by divalent and trivalent cations, and because the Gd^{3+} ions were bound to sites on the $P2X_4$ receptor that might have a role in ion channel function, we asked whether Gd^{3+} altered ATP-dependent receptor gating.

Whole-cell patch-clamp recordings of mammalian tsA201 cells transfected with the $\Delta P2X_4$-A construct demonstrated that in the presence of 100 μM Gd^{3+}, and at a holding potential of −60 mV, coapplication of 30 μM ATP failed to elicit inward current, suggesting that Gd^{3+} is an antagonist (Fig. 5e, f). At positive holding potentials, Gd^{3+} continued to antagonize ATP-dependent receptor activation, thus demonstrating that Gd^{3+} was not acting solely as a pore blocker (Supplementary Fig. 12a). Although increasing ATP concentrations concomitantly extinguished Gd^{3+} antagonism (Supplementary Fig. 12c), raising the possibility that Gd^{3+} might simply sequester ATP, a direct action of Gd^{3+} on the receptor is supported by the fact that preapplication of Gd^{3+} greatly attenuated channel activation when ATP was subsequently applied in a Gd^{3+}-free solution (Supplementary Fig. 12a, b). Furthermore, Gd^{3+} speeds the rate of ion channel deactivation (Supplementary Fig. 12c). Finally, the direct action of Gd^{3+} on the receptor is further bolstered by the presence of four highly occupied Gd^{3+}-binding sites, one of which is at the 'top' of the profoundly acidic central vestibule, a cavity that also serves to attract and concentrate cations (Fig. 5a, g).

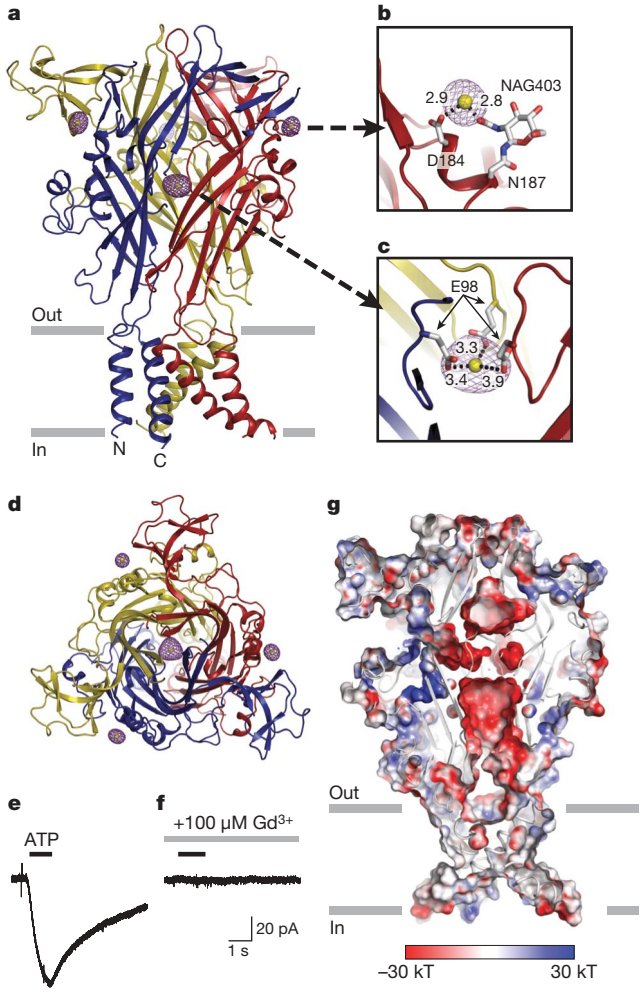

Figure 5 | Gadolinium (Gd^{3+})-binding sites. **a**, Anomalous difference Fourier map contoured at 8.0σ (purple) and the modelled Gd^{3+} ions (yellow). **b**, A peripheral Gd^{3+}-binding site in chain B. Distances between Gd^{3+} and the coordinating carboxyl or hydroxyl groups are shown in angstrom. **c**, The central Gd^{3+}-binding site is coordinated by three Glu 98 residues. **d**, View of the Gd^{3+}-binding sites parallel to the molecular three-fold axis from the extracellular side of the membrane. Panels **a**–**d** are derived from diffraction data measured from crystals of the $\Delta P2X_4$-A construct. **e**, **f**, Gd^{3+} antagonizes $\Delta P2X_4$-EGFP-A whole-cell currents measured by patch-clamp electrophysiology. ATP (30 μM, 1 s, black bar) evokes an inward current in tsA201 cells expressing $\Delta P2X_4$-EGFP-A (**e**). Pre-application of Gd^{3+} (100 μM, 5 s, grey bar) inhibits the current evoked by ATP (30 μM, 1 s, black bar) (**f**). **g**, Acidic surface on the central vestibule of $\Delta P2X_4$. Electrostatic potential surface and cartoon representations of $\Delta P2X_4$-B sliced as in Fig. 4a show an acidic patch located in the middle of the three subunits. The surface is coloured on the basis of the electrostatic potential contoured from −30 kT (red) to +30 kT (blue). White denotes 0 kT. Surface potential was calculated using APBS tools[50] for a $\Delta P2X_4$-B model in which side-chain atoms were added to residues without side-chain atoms in the crystal structure. The following residues were excluded from the calculation: Tyr 53, Asn 78 and Asn 187.

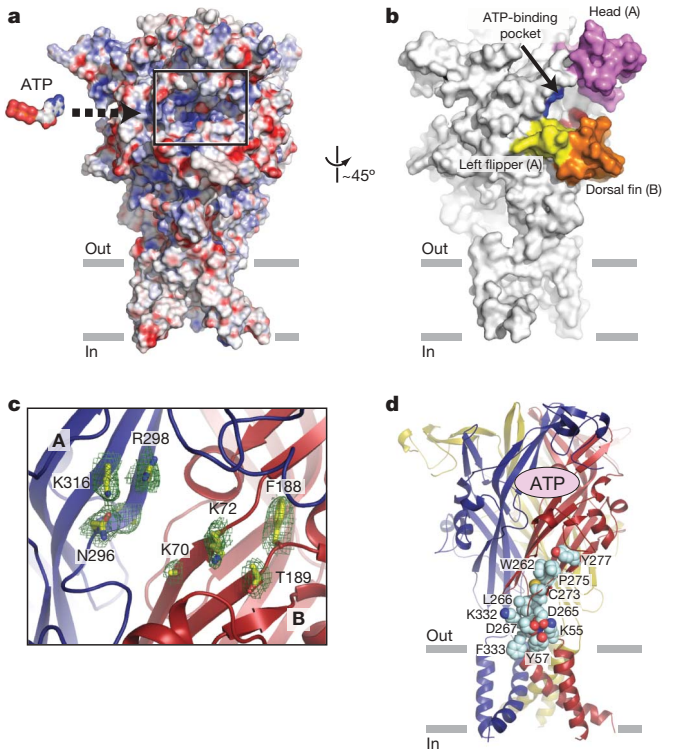

Figure 6 | ATP-binding site. **a**, A plausible ATP-binding pocket located between two neighbouring subunits is highlighted in the black rectangle on an electrostatic potential surface representation of the trimeric $\Delta P2X_4$-B receptor. The surface is coloured on the basis of the electrostatic potential contoured from −30 kT (red) to +30 kT (blue). White denotes 0 kT. An ATP molecule, scaled appropriately, is also shown. **b**, A surface representation viewed ~45° from panel **a**. The head, dorsal fin and left flipper domains forming the jaw-shaped ATP-binding pocket are coloured as in Fig. 3. The putative ATP-binding residues are in blue for subunit A (Asn 296, Arg 298 and Lys 316) and in red for subunit B (Lys 70, Lys 72 and Thr 189). **c**, Close-up view of the highlighted region in **a** illustrating subunits A (blue) and B (red). Conserved residues implicated in ATP binding[42–46] are labelled, and side chains are in stick representation. Contours from a $2F_o - F_c$ electron density map drawn around the side chains are in green. The electron density for the side chain of Lys 70 is weak and it has been built as an alanine. **d**, Conserved residues, shown in space-filling representation, are located between the ATP-binding site and the transmembrane domain–extracellular domain interface. Only residues for a single subunit are shown.

ATP-binding site

The location of the ATP-binding site remains unknown. We suggest that deep grooves on the outside of the trimer, 45 Å from the ion channel domain and spanning neighbouring subunits, are the binding sites for ATP (Fig. 6a, b). These intersubunit grooves are populated by eight conserved residues implicated in ATP-dependent P2X receptor gating[42–46] (Fig. 6c), and whose amino acid composition is compatible with an ATP-binding motif. This putative ATP site, shaped like an open jaw, is one of three in the receptor. It is surrounded by the head domain, the body domain, the right flipper and the dorsal fin, and includes residues Lys 70, Lys 72, Phe 188 and Thr 189 from one subunit, and residues Asn 296, Phe 297, Arg 298 and Lys 316 from the neighbouring subunit. Among those residues, Lys 70, Lys 72, Thr 189, Asn 296, Arg 298 and Lys 316 are oriented towards the groove of the pocket, indicating that they may bind to ATP directly. In contrast, both Phe 188 and Phe 297 are oriented away from the groove, suggesting that they may participate in transducing conformational changes from the binding pocket to the ion channel (Supplementary Fig. 13). We speculate that ATP binding induces movement of the head, right flipper and dorsal fin domains, effectively closing these 'jaws' around the agonist, and thus resulting in conformational changes within and between subunits.

Antagonist-binding site

A recent study has shown that the Phe95Leu mutation in human $P2X_7$ (Ile 94 in zebrafish $P2X_4$) drastically reduces the sensitivity to allosteric antagonists such as N2-(3,4-difluorophenyl)-N1-(2-methyl-5-(1-piperazinylmethyl)phenyl)glycinamide dihydrochloride (GW791343) and 4-(4-fluorophenyl)-2-(4-methylsulphinylphenyl)-5-(4-pyridyl)1H-imidazole[47] (SB203580). Likewise, the Arg126Gly mutation (Ala 126 in zebrafish $P2X_4$) reduces the potency of PPADS. In a different study, Lys 138 in human $P2X_1$ (Asp 141 in

zebrafish $P2X_4$) was shown to be important for the inhibitory effect of suramin[48]. Notably, all residues are located in the vicinity of the predicted ATP-binding pocket. Although speculative, we suggest that these antagonists block conformational rearrangements by occupying part or all of the ATP site and precluding closure of the head, right flipper and dorsal fin domain jaws.

Conclusion

Here we present the first, to our knowledge, crystal structure of an ATP-gated P2X ion channel in a closed, resting state at 3.1 Å resolution, providing atomic-resolution evidence that these receptors are trimeric in subunit stoichiometry, with each subunit being composed of two continuous, transmembrane α-helices, intracellular termini and a large disulphide-bond-rich extracellular domain. We propose that ATP binds to a non-canonical site ~45 Å from the ion channel domain, in a deep cleft, inducing conformational changes within and between subunits. We speculate that these changes, in turn, are propagated to the ion channel by conserved residues located at the interface between the transmembrane domain and the extracellular domain (Fig. 6d), opening the ion channel pore.

METHODS SUMMARY

Thirty-five P2X receptor genes fused to EGFP were separately and rapidly screened by transient transfection in human embryonic kidney (HEK293) cells, followed by FSEC. On the basis of a sharp, symmetric elution profile, the zebrafish $P2X_{4.1}$ receptor was identified as a highly promising construct for X-ray crystallographic studies. The shortest well-behaved constructs of $P2X_{4.1}$ ($\Delta P2X_4$-A or -B) were expressed in Sf9 cells using a baculovirus infection system, the membranes were solubilized in *n*-dodecyl-β-D-maltoside (DDM), and the receptor was purified by metal-ion-affinity and size-exclusion chromatography. $\Delta P2X_4$-A crystals were grown in 10–12% PEG 4000, 100 mM sodium acetate (pH 4.2–4.6), 100 mM ammonium sulphate, and 1 mM $GdCl_3$ in D_2O, whereas $\Delta P2X_4$-B crystals were obtained with 20% PEG 2000, 100 mM Tris, pH 8.4, 300 mM $MgNO_3$ and 1 mM $GdCl_3$. The $\Delta P2X_4$-A structure was solved by SAD using data measured at the gadolinium (Gd) L_{III} edge. SOLVE was used to determine Gd ion positions and to calculate SAD phases. These initial phases were subsequently improved by density modification using programs in the CCP4 package. Iterative model building and refinement were performed using the crystallography software COOT and PHENIX. The $\Delta P2X_4$-B structure was determined by molecular replacement. Whole-cell patch-clamp recordings were performed on tsA201 cells transfected with plasmid DNA encoding $P2X_{4.1}$-EGFP, $\Delta P2X_4$-A-EGFP or $\Delta P2X_4$-B-EGFP constructs.

Full Methods and any associated references are available in the online version of the paper at www.nature.com/nature.

Received 13 February; accepted 4 June 2009.

1. Holton, F. A. & Holton, P. The capillary dilator substances in dry powders of spinal roots; a possible role of adenosine triphosphate in chemical transmission from nerve endings. *J. Physiol. (Lond.)* **126,** 124–140 (1954).
2. Burnstock, G. Purinergic nerves. *Pharmacol. Rev.* **24,** 509–581 (1972).
3. Valera, S. *et al.* A new class of ligand-gated ion channel defined by P_{2x} receptor for extracellular ATP. *Nature* **371,** 516–519 (1994).
4. Lustig, K. D., Shiau, A. K., Brake, A. J. & Julius, D. Expression cloning of an ATP receptor from mouse neuroblastoma cells. *Proc. Natl Acad. Sci. USA* **90,** 5113–5117 (1993).
5. Webb, T. E. *et al.* Cloning and functional expression of a brain G-protein-coupled ATP receptor. *FEBS Lett.* **324,** 219–225 (1993).
6. Brake, A. J., Wagenbach, M. J. & Julius, D. New structural motif for ligand-gated ion channels defined by an ionotropic ATP receptor. *Nature* **371,** 519–523 (1994).
7. Schwiebert, E. M. & Zsembery, A. Extracellular ATP as a signaling molecule for epithelial cells. *Biochim. Biophys. Acta* **1615,** 7–32 (2003).
8. Surprenant, A. & North, R. A. Signaling at purinergic P2X receptors. *Annu. Rev. Physiol.* **71,** 333–359 (2008).
9. Khakh, B. S. & Henderson, G. ATP receptor-mediated enhancement of fast excitatory neurotransmitter release in the brain. *Mol. Pharmacol.* **54,** 372–378 (1998).
10. Gu, J. G. & MacDermott, A. B. Activation of ATP P2X receptors elicits glutamate release from sensory neuron synapses. *Nature* **389,** 749–753 (1997).
11. Hugel, S. & Schlichter, R. Presynaptic P2X receptors facilitate inhibitory GABAergic transmission between cultured rat spinal cord dorsal horn neurons. *J. Neurosci.* **20,** 2121–2130 (2000).
12. Donato, R. *et al.* GABA release by basket cells onto Purkinje cells, in rat cerebellar slices, is directly controlled by presynaptic purinergic receptors, modulating Ca^{2+} influx. *Cell Calcium* **44,** 521–532 (2008).
13. Edwards, F. A., Gibb, A. J. & Colquhoun, D. ATP receptor-mediated synaptic currents in the central nervous system. *Nature* **359,** 144–147 (1992).
14. Sim, J. A. *et al.* Altered hippocampal synaptic potentiation in $P2X_4$ knock-out mice. *J. Neurosci.* **26,** 9006–9009 (2006).
15. Finger, T. E. *et al.* ATP signaling is crucial for communication from taste buds to gustatory nerves. *Science* **310,** 1495–1499 (2005).
16. Cook, S. P., Vulchanova, L., Hargreaves, K. M., Elde, R. & McCleskey, E. W. Distinct ATP receptors on pain-sensing and stretch-sensing neurons. *Nature* **387,** 505–508 (1997).
17. Souslova, V. *et al.* Warm-coding deficits and aberrant inflammatory pain in mice lacking $P2X_3$ receptors. *Nature* **407,** 1015–1017 (2000).
18. Cockayne, D. A. *et al.* Urinary bladder hyporeflexia and reduced pain-related behaviour in $P2X_3$-deficient mice. *Nature* **407,** 1011–1015 (2000).
19. Chessell, I. P. *et al.* Disruption of the $P2X_7$ purinoceptor gene abolishes chronic inflammatory and neuropathic pain. *Pain* **114,** 386–396 (2005).
20. Yamamoto, K. *et al.* Impaired flow-dependent control of vascular tone and remodeling in P2X4-deficient mice. *Nature Med.* **12,** 133–137 (2006).
21. Inscho, E. W., Cook, A. K., Imig, J. D., Vial, C. & Evans, R. J. Renal autoregulation in $P2X_1$ knockout mice. *Acta Physiol. Scand.* **181,** 445–453 (2004).
22. Solle, M. *et al.* Altered cytokine production in mice lacking $P2X_7$ receptors. *J. Biol. Chem.* **276,** 125–132 (2001).
23. White, N. & Burnstock, G. P2 receptors and cancer. *Trends Pharmacol. Sci.* **27,** 211–217 (2006).
24. Di Virgilio, F. Liaisons dangereuses: $P2X_7$ and the inflammasome. *Trends Pharmacol. Sci.* **28,** 465–472 (2007).
25. North, R. A. Molecular physiology of P2X receptors. *Physiol. Rev.* **82,** 1013–1067 (2002).
26. Aschrafi, A., Sadtler, S., Niculescu, C., Rettinger, J. & Schmalzing, G. Trimeric architecture of homomeric $P2X_2$ and heteromeric $P2X_{1+2}$ receptor subtypes. *J. Mol. Biol.* **342,** 333–343 (2004).
27. Barrera, N. P., Ormond, S. J., Henderson, R. M., Murrell-Lagnado, R. D. & Edwardson, J. M. Atomic force microscopy imaging demonstrates that $P2X_2$ receptors are trimers but that $P2X_6$ receptor subunits do not oligomerize. *J. Biol. Chem.* **280,** 10759–10765 (2005).
28. Nicke, A. *et al.* $P2X_1$ and $P2X_3$ receptors form stable trimers: a novel structural motif of ligand-gated ion channels. *EMBO J.* **17,** 3016–3028 (1998).
29. Nicke, A., Rettinger, J. & Schmalzing, G. Monomeric and dimeric byproducts are the principal functional elements of higher order $P2X_1$ concatamers. *Mol. Pharmacol.* **63,** 243–252 (2003).
30. North, R. A. & Surprenant, A. Pharmacology of cloned P2X receptors. *Annu. Rev. Pharmacol. Toxicol.* **40,** 563–580 (2000).
31. Kellenberger, S. & Schild, L. Epithelial sodium channel/degenerin family of ion channels: a variety of functions for a shared structure. *Physiol. Rev.* **82,** 735–767 (2002).
32. Kawate, T. & Gouaux, E. Fluorescence-detection size-exclusion chromatography for precrystallization screening of integral membrane proteins. *Structure* **14,** 673–681 (2006).
33. Diaz-Hernandez, M. *et al.* Cloning and characterization of two novel zebrafish P2X receptor subunits. *Biochem. Biophys. Res. Commun.* **295,** 849–853 (2002).
34. Blake, C. C., Geisow, M. J., Oatley, S. J., Rerat, B. & Rerat, C. Structure of prealbumin: secondary, tertiary and quaternary interactions determined by Fourier refinement at 1.8 Å. *J. Mol. Biol.* **121,** 339–356 (1978).
35. Williams, D. C. Jr, Lee, J. Y., Cai, M., Bewley, C. A. & Clore, G. M. Crystal structures of the HIV-1 inhibitory cyanobacterial protein MVL free and bound to Man3GlcNAc2: structural basis for specificity and high-affinity binding to the core pentasaccharide from n-linked oligomannoside. *J. Biol. Chem.* **280,** 29269–29276 (2005).
36. Ennion, S. J. & Evans, R. J. Conserved cysteine residues in the extracellular loop of the human $P2X_1$ receptor form disulfide bonds and are involved in receptor trafficking to the cell surface. *Mol. Pharmacol.* **61,** 303–311 (2002).
37. Clyne, J. D., Wang, L. F. & Hume, R. I. Mutational analysis of the conserved cysteines of the rat $P2X_2$ purinoceptor. *J. Neurosci.* **22,** 3873–3880 (2002).
38. Fabbretti, E. *et al.* Identification of negative residues in the $P2X_3$ ATP receptor ectodomain as structural determinants for desensitization and the Ca^{2+}-sensing modulatory sites. *J. Biol. Chem.* **279,** 53109–53115 (2004).
39. Duckwitz, W., Hausmann, R., Aschrafi, A. & Schmalzing, G. $P2X_5$ subunit assembly requires scaffolding by the second transmembrane domain and a conserved aspartate. *J. Biol. Chem.* **281,** 39561–39572 (2006).
40. Li, M., Chang, T. H., Silberberg, S. D. & Swartz, K. J. Gating the pore of P2X receptor channels. *Nature Neurosci.* **11,** 883–887 (2008).
41. Gonzales, E. B., Kawate, T. & Gouaux, E. Pore architecture and ion sites in acid-sensing ion channels and P2X receptors. *Nature* doi:10.1038/nature08218 (this issue).
42. Ennion, S., Hagan, S. & Evans, R. J. The role of positively charged amino acids in ATP recognition by human $P2X_1$ receptors. *J. Biol. Chem.* **275,** 29361–29367 (2000).
43. Roberts, J. A. & Evans, R. J. ATP binding at human $P2X_1$ receptors. Contribution of aromatic and basic amino acids revealed using mutagenesis and partial agonists. *J. Biol. Chem.* **279,** 9043–9055 (2004).
44. Jiang, L. H., Rassendren, F., Surprenant, A. & North, R. A. Identification of amino acid residues contributing to the ATP-binding site of a purinergic P2X receptor. *J. Biol. Chem.* **275,** 34190–34196 (2000).

45. Roberts, J. A. & Evans, R. J. Contribution of conserved polar glutamine, asparagine and threonine residues and glycosylation to agonist action at human $P2X_1$ receptors for ATP. *J. Neurochem.* **96,** 843–852 (2006).
46. Marquez-Klaka, B., Rettinger, J., Bhargava, Y., Eisele, T. & Nicke, A. Identification of an intersubunit cross-link between substituted cysteine residues located in the putative ATP binding site of the P2X1 receptor. *J. Neurosci.* **27,** 1456–1466 (2007).
47. Michel, A. D. *et al.* Identification of regions of the $P2X_7$ receptor that contribute to human and rat species differences in antagonist effects. *Br. J. Pharmacol.* **155,** 738–751 (2008).
48. Sim, J. A., Broomhead, H. E. & North, R. A. Ectodomain lysines and suramin block of $P2X_1$ receptors. *J. Biol. Chem.* **283,** 29841–29846 (2008).
49. Smart, O. S., Goodfellow, J. M. & Wallace, B. A. The pore dimensions of gramicidin A. *Biophys. J.* **65,** 2455–2460 (1993).
50. Baker, N. A., Sept, D., Joseph, S., Holst, M. J. & McCammon, J. A. Electrostatics of nanosystems: application to microtubules and the ribosome. *Proc. Natl Acad. Sci. USA* **98,** 10037–10041 (2001).

Supplementary Information is linked to the online version of the paper at www.nature.com/nature.

Acknowledgements We thank the personnel at beamlines 5.0.2, 8.2.1 and 8.2.2 of the Advanced Light Source and at beamline 24-ID-E of the Advanced Photon Source. We also thank M. Voigt for zebrafish P2X receptor DNA, T. Homrichhausen for help with cloning and FSEC screening, J. Berriman for help with electron microscopy, L. Vaskalis for assistance with illustrations, and Gouaux laboratory members for discussions. This work was supported by the National Institutes of Health (NIH) and the American Asthma Foundation. E.G. is an investigator with the Howard Hughes Medical Institute.

Author Contributions E.G. and T.K. designed the project. T.K. performed cloning, cell culture, FSEC screening, purification, characterization, electron microscopy and crystallography. J.C.M. performed cloning, cell culture, FSEC screening, purification and crystallization. W.T.B. carried out the electrophysiology. All authors contributed to writing the manuscript.

Author Information Atomic coordinates and structure factors have been deposited with the Protein Data Bank under codes 3I5D and 3H9V for the $\Delta P2X_4$-A and $\Delta P2X_4$-B constructs, respectively. Reprints and permissions information is available at www.nature.com/reprints. Correspondence and requests for materials should be addressed to E.G. (gouauxe@ohsu.edu).

METHODS

Expression and purification. The shortest well-behaved construct of zebrafish $P2X_{4.1}$ ($\Delta P2X_4$-A)[51,52] was determined by examining twelve different combinations of N and C termini deletions in Sf9 cells by rapid FSEC analysis. Similarly, the FSEC screening strategy was exploited to identify a well-behaved derivative of $\Delta P2X_4$-A that carries mutations at two of four glycosylation sites (Asn78Lys/Asn187Arg) and a point mutation (Cys51Phe) in TM1 ($P2X_4$-B). The $\Delta P2X_4$-A protein was expressed as an N-terminal EGFP fusion with an octa-histidine affinity tag (EGFP–8×His) in baculovirus-infected Sf9 cells. Infected Sf9 cells were cultured in serum-free medium (Invitrogen) at 27 °C for 24 h after infection, after which time the temperature was reduced to 20 °C. Cells were collected 72 h after infection by centrifugation at 6,200*g* and broken by sonication in TBS (50 mM Tris, pH 8.0, 150 mM NaCl) supplemented with 1 mM phenylmethanesulphonylfluoride, 5.2 μg ml^{-1} aprotinin, 2 μg ml^{-1} leupeptin, and 1.4 μg ml^{-1} pepstatin A (all from Sigma Aldrich). Cell debris was cleared by a low-speed spin (10,000*g*). Membranes were collected by a high-speed spin (19,000*g*) and solubilized in TBS containing 40 mM DDM (Anatrace). The detergent-soluble fraction was incubated with cobalt-charged metal ion affinity resin (Clontech), and $\Delta P2X_4$ was eluted with 250 mM imidazole (Fluka) and 1 mM DDM in TBS. After thrombin digestion to remove the EGFP–8×His tag, $\Delta P2X_4$ was isolated by size-exclusion chromatography in 20 mM HEPES, pH 7.0, 80 mM NaCl, 20 mM KCl and 0.5 mM DDM. Peak fractions were pooled, concentrated to 2 mg ml^{-1}, and used for crystallization. All steps after Sf9 cell culture were carried out on ice or at 4 °C. For the purification of $\Delta P2X_4$-B, all steps were identical with the exception that 15% glycerol was included in the solubilization, metal-ion affinity and size-exclusion chromatography buffers. For production of selenomethionine (SeMet)-labelled receptor, baculovirus-infected Sf9 cells were cultured for 1 day at 27 °C, collected by centrifugation at 1,000*g* for 5 min, re-cultured in serum-free medium without methionine for 4 h at 27 °C, and then supplemented with 50 mg l^{-1} SeMet (Anatrace). After 10 h incubation at 27 °C, the temperature was shifted to 20 °C, and the cells were cultured for another 2 days before collection. SeMet proteins were purified as described earlier.

Crystallization. For $\Delta P2X_4$-A, crystals were obtained at 4 °C in 3–4 weeks by vapour diffusion by mixing 1:1 or 2:1 (v/v) ratios of protein and a reservoir solution containing 10–12% PEG 4000, 100 mM sodium acetate (pH 4.2–4.6), 100 mM ammonium sulphate and 1 mM $GdCl_3$ in D_2O. Crystals were dehydrated and cryoprotected by adding glycerol in 2.5% steps (final 12.5%) followed by increasing the PEG 4000 concentration by 2.5% steps (final 25%). For native and SeMet crystals, $GdCl_3$ was excluded from the final cryoprotection solution. For $\Delta P2X_4$-B, crystals were obtained at 4 °C in 9 months by vapour diffusion by mixing 1:1 or 2:1 ratios of protein and a reservoir solution containing 20% PEG 2000, 300 mM $Mg(NO_3)_2$, 100 mM Tris, pH 8.4, and 1 mM $GdCl_3$. Crystals were cryoprotected by adding glycerol in 2.0% steps (final 18%). Crystals were flash-frozen in liquid nitrogen and used for X-ray diffraction data collection.

Structure determination. X-ray data sets were collected at the Advanced Light Source (beam lines 5.0.2, 8.2.1 and 8.2.2) and at the Advanced Photon Source (beamline 24-ID-E). The diffraction frames were indexed, integrated and scaled using HKL2000. The structure of $\Delta P2X_4$-A was solved using data from a SAD experiment (Advanced Light Source beamline 5.0.2). The program SOLVE was used to find heavy-atom positions and to calculate phases. The phases were improved by density modification that included three-fold non-crystallographic symmetry averaging, as carried out by the computer program DM. This *R*3 space group crystal form has one receptor trimer in the asymmetric unit (Supplementary Fig. 4). Initially, several poly-alanine chains were built into the electron density map using COOT. Subsequently, specific protein sequences, together with correct side-chain atoms, were fitted to the electron density map on the basis of Met and Cys locations derived from anomalous Fourier difference maps calculated from SeMet data derived from wild-type, Cys51Met or Leu349Met constructs (Supplementary Fig. 5) and from native data collected at a low energy ($\lambda = 1.6$ Å), respectively. Finally, iterative model building using COOT and CCP4 led to a continuous protein model that nevertheless contained several Ala residues at positions where the native, longer amino acid side chains were disordered. The resulting structure was manually rebuilt and refined using programs in the CCP4, COOT and PHENIX packages with the following NCS restraints: B-factor weight, 10; coordinate sigma, 0.1 for residues 36–64, 119–169 and 326–352, and 0.04 for residues 65–118 and 170–235. The structure of $\Delta P2X_4$-B was obtained by molecular replacement with the refined model of $\Delta P2X_4$-A using the program Phaser. There is one subunit in the asymmetric unit of the *R*32 $\Delta P2X_4$-B crystal form. The resulting model was manually rebuilt and refined using programs in the CCP4, COOT and PHENIX packages. Electron densities for the transmembrane helices 1 and 2 are shown in Supplementary Fig. 6. The structures were validated by the computer program PROCHECK and MolProbity.

Electrophysiology. Whole-cell patch-clamp experiments were performed on a mammalian cell line (tsA201) transiently expressing EGFP, $P2X_{4.1}$-EGFP, $\Delta P2X_4$-A-EGFP or $\Delta P2X_4$-B-EGFP constructs using methods previously described. The holding potential was −70 mV unless noted. The pipette solution contained (in mM): 115 K-methanesulphonate, 20 NaCl, 1.5 $MgCl_2$, 10 HEPES and 10 BAPTA; pH was adjusted to 7.4 with KOH. Standard extracellular solution contained (mM): 140 NaCl, 5 KCl, 2 $CaCl_2$, 1 $MgCl_2$, 10 HEPES and 10 MES; pH was adjusted to 7.4 using *N*-methyl-D-glucamine. ATP test solutions were made from serial dilutions of standard extracellular solution supplemented with 10 mM Na_2ATP, pH 7.4, with *N*-methyl-D-glucamine. Dilutions were made in standard extracellular solution supplemented with 20 mM NaCl to maintain an equivalent sodium concentration among all test solutions. External solutions were exchanged on cells within 20 ms using computer actuated solenoid valves controlling flow through an array of 10 μl pipettes positioned within several hundred micrometres of the cell. All recordings were at room temperature (~23 °C). Data were collected using pClamp (Molecular Devices), analysed with Clampfit (Molecular Devices) and Origin Lab software, and organized using Excel (Microsoft). To account for run-down of current responses, the peak current amplitude for each ATP test was measured and scaled relative to the current evoked by a preceding test of 100 μM ATP (a concentration which did not cause run-down). Data were plotted relative to the current evoked by 100 μM ATP and fit to the Hill equation to determine the ATP concentration required to evoke a half-maximal current. For presentation, data were normalized to the maximum-evoked current (I_{max}) of the best fit to the Hill equation.

51. Diaz-Hernandez, M. *et al.* Cloning and characterization of two novel zebrafish P2X receptor subunits. *Biochem. Biophys. Res. Commun.* **295**, 849–853 (2002).
52. Kucenas, S. *et al.* Molecular characterization of the zebrafish P2X receptor subunit gene family. *Neuroscience* **121**, 935–945 (2003).